


FULL PAPER

Open Access



# Analog field-scale acoustic study of volcanic eruption directivity using a tiltable liquid nitrogen-charged water cannon

Arthur D. Jolly<sup>1,2\*</sup> , Ben Kennedy<sup>3</sup>, Robin S. Matoza<sup>4</sup>, Alexandra M. Iezzi<sup>4,8</sup>, Bruce Christenson<sup>5</sup>, Richard Johnson<sup>6</sup>, Amilea Sork<sup>3</sup> and David Fee<sup>7</sup>

## Abstract

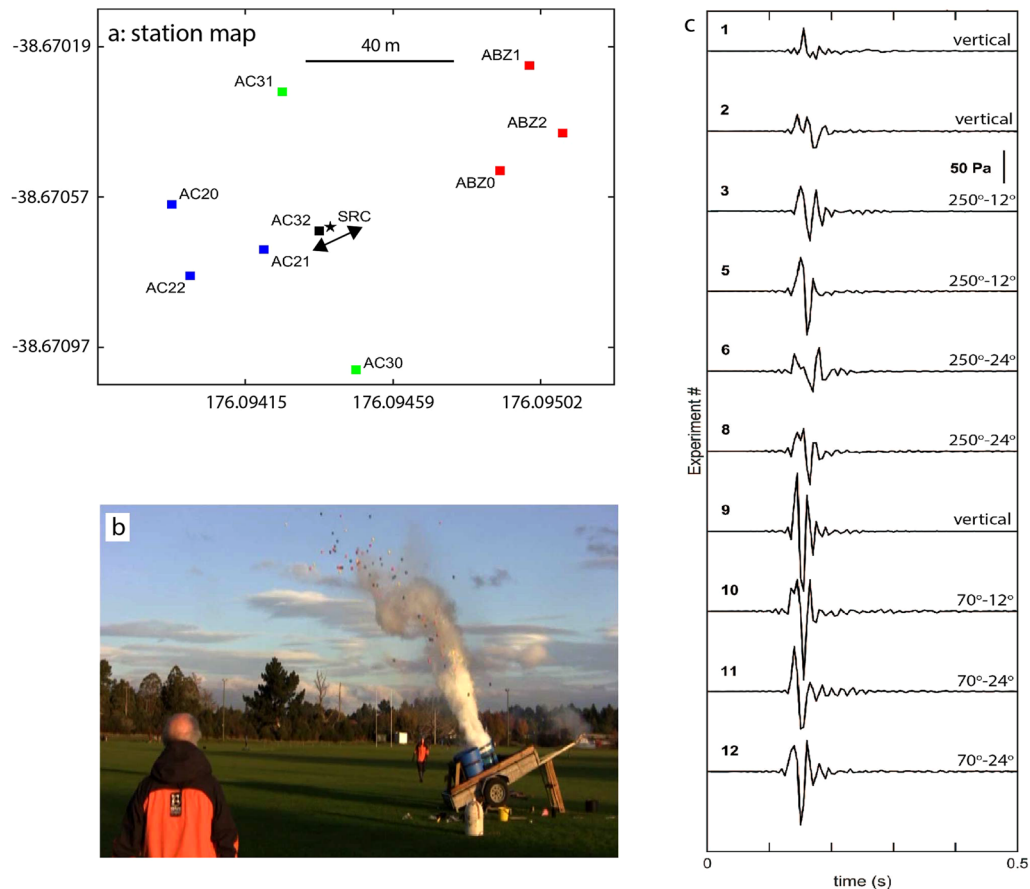
Laterally directed explosive eruptions are responsible for multiple fatalities over the past decade and are an increasingly important volcanology problem. To understand the energy dynamics for these events, we collected field-scale explosion data from nine acoustic sensors surrounding a tiltable cannon as part of an exploratory experimental design. For each cannon discharge, the blast direction was varied systematically at 0°, 12°, and 24° from vertical, capturing acoustic wavefield directivity related to the tilt angle. While each event was similar in energy discharge potential, the resulting acoustic signal features were variable event-to-event, producing non-repetitious waveforms and spectra. Systematic features were observed in a subset of individual events for vertical and lateral discharges. For vertical discharges, the acoustic energy had a uniform radiation pattern. The lateral discharges showed an asymmetric radiation pattern with higher frequencies in the direction of the blast and depletion of those frequencies behind the cannon. Results suggest that, in natural volcanic systems, near-field blast directionality may be elucidated from acoustic sensors in absence of visual data, with implications for volcano monitoring and hazard assessment.

**Keywords:** Volcanic eruptions, Lateral blast, Source dynamics, Source processes, Volcano acoustics, Directivity, Directionality, Doppler shift, Waveform template clustering, Source evolution

\*Correspondence: [ajolly@usgs.gov](mailto:ajolly@usgs.gov)

<sup>1</sup> U.S. Geological Survey, Hawaiian Volcano Observatory, Suite A8, 1266 Kamehameha Avenue, Hilo, HI 96720, USA  
Full list of author information is available at the end of the article

## Graphical Abstract



## Introduction

Small-scale volcanic eruptions from phreatic to Strombolian systems are especially important from a hazard and impact perspective. While such systems produce very small eruptions and small hazard footprints and magnitudes, they pose out-sized risks due to the exposure of sightseers to these frequent events (Erfurt-Cooper 2014; Fitzgerald et al. 2017). Visitors are often attracted to these beautiful landscapes, unusual hydrothermal features and the exciting small-scale eruptive activity. Such volcanic systems may appear to be safe, and decades may pass without an event that impacts visitors (Kilgour et al. 2021). However, small departures from the usual activity are possible, represented either by a small increase in eruption size, or due to a vent system change that may locally increase the chance of a lateral mass flow or directed blast. Either process may have significant hazard/impact consequences to near vent visitors.

Eruptive directionality for small-scale systems have been increasingly observed in the past decade, due to improved observational capabilities from the global

volcano monitoring community. Phreatic and phreatomagmatic eruptions at Ruapehu (Kilgour et al. 2010; Jolly et al. 2010), Te Maari (Lube et al. 2014; Jolly et al. 2014; Fitzgerald et al. 2014), and Ontake (Tsunematsu et al. 2016; Takarada et al. 2016) have all revealed significant hazards from lateral eruption events that have produced infrastructure damage or injuries and fatalities. Recent studies at Strombolian systems have also documented eruption directionality as evidenced by infrasound and ballistic mapping at Yasur volcano, Vanuatu (e.g., Jolly et al. 2017; Iezzi et al. 2019; Fitzgerald et al. 2020). Lateral directionality is not confined to small eruptions, however. Indeed, the 1980 Mount St. Helens blast (Kieffer 1981; Kanamori and Given 1982) produced significant lateral blast products from the syn-eruptive landslide event.

Eruption directionality is analogous to earthquake directivity and may suggest common wavefield propagation features. For a large earthquake, directivity results from rupture propagation within the fault plane which can produce variable waveform amplitude and spectral characteristics towards and away from the primary

rupture direction (e.g., Eberhart-Phillips et al. 2003; Abercrombie et al. 2017) on a surrounding seismic network. Anthropogenic sources also may produce directivity/directionality features. In volcano observatory settings, helicopter or fixed wing aircraft (e.g., Hubbard et al. 1971) are often observed in seismic and acoustic records as tremor like signals having highly variable peak frequencies consistent with the Doppler spectral shift (Eibl et al. 2015).

Ballistic and ash particles, which may produce acoustic waves through turbulent interaction with surrounding air (Matoza et al. 2013; Rowell et al. 2014) can produce extended sources that may be recorded on nearby sensors. In this case, the excitations produced by the ash/ballistic mass may impart different frequency contents to a stationary observation point towards or away from the direction of eruption mass propagation. Consistent with this theory, one might expect to observe lower frequency signals for an acoustic sensor positioned behind the direction of propagation, and generally higher frequencies for a sensor in the direction of mass flow.

In this contribution, we complete an initial controlled field-scale laboratory experiment where we attempt to create directionality features of vertical and laterally directed explosions. We aim to establish field conditions that emulate those captured by a set of acoustic sensors in the near-field (where the source dimension is large compared to the observation array) volcanic environment while controlling important features of an eruption, including the event size, source response and discharge direction, such that waveform features and spectral characteristics can be monitored. The eruption conditions emulated here are mixed liquid–gas jets (e.g., Zhang et al. 2016) that are akin to eruptions through volcanic lakes (e.g., Kilgour et al. 2010; Jolly et al. 2010; Fee et al. 2020; Lyons et al. 2019), and may be dynamically different from ash–gas jets from dry bed volcanic systems. Regardless, by controlling the eruption parameters, we aim to determine which characteristic features may be identified for real volcanic eruptions, to improve eruption source characterization and inform volcano monitoring decisions.

Results of this exploratory experiment show that efforts to control the source process were only partially successful as shown by the variations in waveforms event-to-event. However, a subset of the highest energy explosions suggests that the acoustic impulse response from an artificial eruption imparts distinct spectral signatures that may emulate features of natural volcanic eruptions. The work provides a framework for improvement of future experiments of this class.

## Experimental setup

We developed an experimental apparatus (Fig. 1) to produce directed explosions consistent with a prior field experimental eruption approach (Wadsworth et al. 2018). The setup included a 209-L steel barrel (diameter 572 mm and height 851 mm) partially filled to  $\sim 1/3$  capacity with water at approximately ambient temperature. For each experiment a light-duty plastic bottle (1.5-L emptied soda-pop bottle) was filled to  $\sim 1/4$  with liquid nitrogen ( $N_2$ ), sealed with the cap, and immersed into the water. The process of immersion produced heating and gas expansion within the bottle which increased the internal bottle pressure. The bottles tensile strength was eventually exceeded, causing bottle rupture and rapid expansion and vaporization of the liquid nitrogen. Our experimental design avoided the expense and logistical complexity of chemical explosive experiments (e.g., Goto, et al. 2001; Bowman et al. 2014; Sonder et al. 2022) allowing the generation of multiple example events over a relatively short period.

The resulting explosion was directed through the open end of the barrel (the vent) causing a directed blast of the water/liquid nitrogen mixture. The barrel was secured on a small truck trailer and the bottle was secured to the base of the barrel by a heavy mass with duct tape holding the immersed bottle in place (Fig. 1b, c). The barrel angle from vertical was adjustable via the natural angle of the trailer tow structure (Fig. 1d) augmented by stable wood support which in our case, allowed the explosion direction to be variably adjusted. Experiments included discharge angles of  $\sim 0^\circ$ ,  $12^\circ$  and  $24^\circ$  from vertical and azimuths northeast ( $70^\circ$ ) and southwest ( $250^\circ$ ) from true north. The experiment occurred on 3 March 2016 at Owen Delany Park in Taupo, New Zealand. Mild weather conditions were available with temperatures  $\sim 18^\circ\text{C}$  and light variable winds that did not exceed  $\sim 4\text{ m/s}$ . A total of 12 experiments were attempted (Table 1), over a 2.5-h period.

Data were collected using 9 infraBSU infrasound sensors (Marcillo et al. 2012) surrounding the apparatus at ranges of 2–70 m (Fig. 1a and Table 1) from the source. The acoustic data were collected on 3 DiGOS DATA CUBE digitizers recording at 200 Hz with cables to each sensor. The sensors had a flat response from 0.033 to 200 Hz and GPS locations were known to within  $\sim 5\text{ m}$ . The sensors were deployed to surround the cannon source position: three were positioned northeast of the source (ABZ0, ABZ1, ABZ2), three southwest of the source (AC20, AC21, AC22), two laterally on either side of the rotatable cannon (AC30, AC31) and one sensor (AC32) was located beneath the trailer (within  $\sim 2\text{ m}$  of the base of the cannon source position-SRC). A summary of the field setup is shown in Fig. 1a and Tables 1

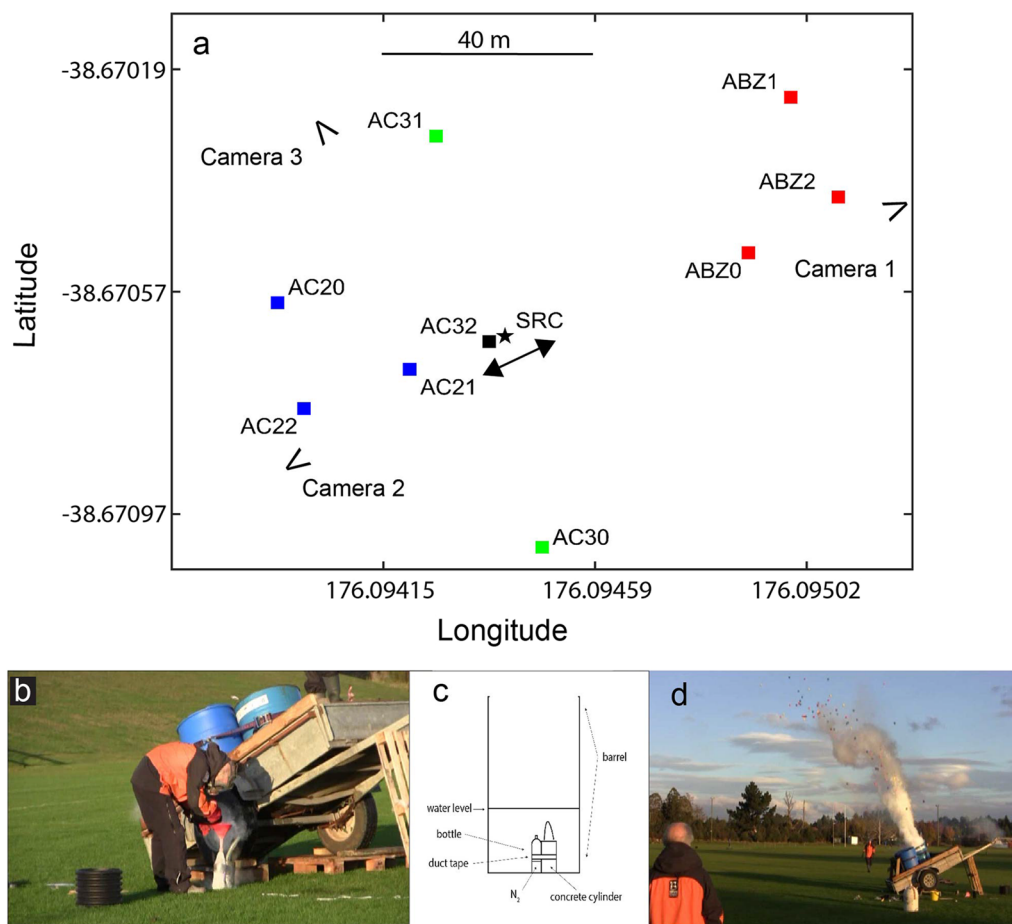


**Fig. 1** Map (a) showing experimental setup and distribution of sensors (squares colored red for northeast sensors, blue for southwest sensors, green for sensors lateral to the discharge direction and black for a sensor under the cannon). The angled blast direction is shown by the black double arrow. Latitude and longitude are given in decimal degrees. Cameras (V open to the look direction) documented 10 successful discharges. The black star shows the cannon. For each experiment, the bottle (b) was partially filled with liquid-nitrogen, sealed with the cap and placed in the partially water filled barrel (see “Experimental setup” section). Diagram showing the discharge apparatus within the barrel shown in c. An example discharge (d) for Experiment 11 yielded a lateral discharge of a water/nitrogen mixture. Colored balls aided assessment of discharge exit velocities. Images (b, c) are from video captures generated by Julian Thompson (GNS Science)

and 2. Video was recorded by three GoPro Hero 3 cameras, orthogonally oriented to the eruption to capture directionality and exit velocity. The GoPro cameras recorded at 30 frames per second and individual frames were extracted from the videos. In most cases, color was inverted to improve contrast, and the parabolic paths of balls with tracks most orthogonal to the camera angle were measured individually to get maximum velocities and heights (see Table 3 and supplementary videos). Evening lighting and camera resolution provided some challenges with detailed tracking analysis. The measurements presented here focused on camera 2 and a comparison between experiment 9 (vertical explosion) and experiment 12 (the 24° northeastward

directed experiment). For this reason, only partial tracks for several ballistics were analyzed. Additionally, the velocity of the vaporized water and liquid nitrogen was tracked for these two experiments.

For infrasound sensors, we synchronized the data timing, corrected the data to pressure, extracted individual events and computed the spectra using standard fast Fourier transform (FFT) over a 200 sample (1 s) window drawn from the unfiltered record. All waveforms are available as part of an online data release (see “Availability of data and materials” section).

**Table 1** Experiment results

N	Event time (UTC) <sup>a</sup>	Azimuth <sup>b</sup>	Blast angle <sup>c</sup>	Pressure (Pa) <sup>d</sup>	Comment <sup>e</sup>
1	02:26:45	Vertical	0°	28.8	L&P
2	02:35:49	Vertical	0°	20.9	L&P
<b>3</b>	<b>02:47:41</b>	<b>250°</b>	<b>12°</b>	<b>31.2</b>	<b>L&amp;P</b>
4					Failed discharge
<b>5</b>	<b>03:26:24</b>	<b>250°</b>	<b>12°</b>	<b>42.3</b>	<b>L&amp;P</b>
6	03:51:41	250°	24°	29.4	L&P
7					Failed discharge
8	04:13:48	250°	24°	28.6	MY
<b>9</b>	<b>04:21:40</b>	<b>Vertical</b>	<b>0°</b>	<b>72.7</b>	<b>MY</b>
<b>10</b>	<b>04:35:04</b>	<b>70°</b>	<b>12°</b>	<b>39.8</b>	<b>MY</b>
<b>11</b>	<b>04:50:12</b>	<b>70°</b>	<b>24°</b>	<b>56.1</b>	<b>MY</b>
<b>12</b>	<b>04:57:21</b>	<b>70°</b>	<b>24°</b>	<b>38.6</b>	<b>MY</b>

Bold denotes interpreted experiments

<sup>a</sup> Experiment date is 3 May 2016 14:26–16:57 NZST (3 May 2016 2:26–4:57 UTC)

<sup>b</sup> Measured clockwise from north

<sup>c</sup> Measured from vertical

<sup>d</sup> Peak positive pressure measured from beneath the explosion source

<sup>e</sup> Bottle type detonated: (L&P) brown soft-drink bottles, (MY) clear soft-drink bottles

**Table 2** Station and cannon (SRC) latitude and longitude locations given in decimal degrees

Station	Easting (m)	Northing (m)	Elevation (m)	Distance (m)	Azimuth (degrees)	Comment
SRC	− 38.67065	176.09436	395	0		Source position
AC30	− 38.67098	176.09450	398	39	170	Lateral from source
AC31	− 38.67032	176.09423	396	38	340	Lateral from source
AC32	− 38.67065	176.09436	395	3	251	Under source
AC20	− 38.67060	176.09390	391	43	278	Southwest of source
AC21	− 38.67070	176.09419	392	19	252	Southwest of source
AC22	− 38.67077	176.09397	392	40	251	Southwest of source
ABZ0	− 38.67049	176.09492	398	48	72	Northeast of source
ABZ1	− 38.67024	176.09500	400	69	51	Northeast of source
ABZ2	− 38.67040	176.09511	400	67	58	Northeast of source

**Table 3** Eruption description

	Max. measured vapor velocity (m/s)	Max. measured vapor height (m)	Max measured ball velocity (m/s)	Max measured ball height (m) <sup>a</sup>	Explosion description
Exp 9 (vertical)	60 ( $n = 2$ )	6.3	12.2–15.3 ( $n = 5$ )	9.4	Vapor jet narrow vertical explosion, most balls went height and landed close to barrel, slight asymmetric distribution (northeast)
Exp12 (24°)	28.3 ( $n = 3$ )	5.1	10.6–21.7 ( $n = 7$ )	4.5	Fanned vapor jet, balls landed farther from barrel strongly asymmetric distribution (northeast)

<sup>a</sup> Measured from base of explosion above ground

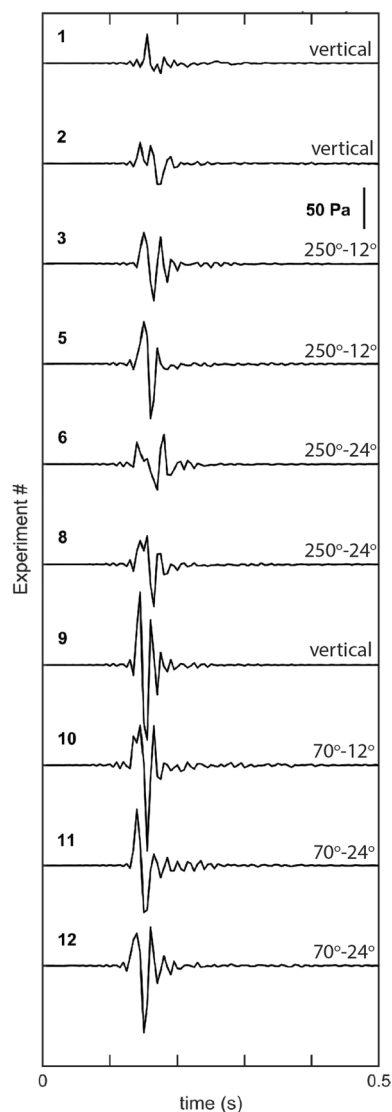


**Fig. 2** Example discharges from sensor AC32 located under the source (SRC). Each discharge is labeled as described in Table 2. Note the highly variable waveform characteristics event-to-event. The window onset is  $\sim 0.1$  s prior to the explosion onset for each experiment

## Results

For the 12 experiments attempted, two failed to discharge due to slow bottle cap leakage (Table 1). Each of the 10 successful explosions was recorded on the 9-element ground network; however, Experiment 10 occurred during a very short data gap for sensor AC20 and that data was excluded from the analysis. For the successful discharges, three primary issues were noted. First, we found that the waveform data may have been under-sampled (Fig. 2) related to the 200-Hz data rate. Hence, the full wave features and spectral content of

the discharges may not be fully captured. Second, a subset of the explosions had insufficient energy release based on the measured peak pressure at the near cannon sensor (AC32). Table 1 shows that the peak pressure at AC32 for the experiment ranged from 20.9 to 72.7 Pa (Fig. 2), but the aforementioned under-sampling implies that the true peak pressures may be higher. Inspection of the wider waveform and spectral data shows that the smaller events had significant low frequency noise (Figs. 3, 4, 5). Third, Experiments 1, 2 and 6 produced complex spectral patterns (Figs. 4a, c, 5a) which were difficult to interpret.

With these issues, we limited the interpretation to events having peak pressures above 30 Pa at the near source station (AC32) and we did not interpret observations for events having multiple spectral peaks. Application of these criteria left 6 events (3, 5, 9–12) for subsequent analysis. The subset of events included one vertical discharge, three northeast-directed discharges, and two southwest directed discharges. Unfortunately, the southwest directed discharges did not include a high lateral angle example, limiting their value for the interpretation of lateral directionality. For completeness, we include all examples in (Figs. 4, 5).

The selected events yielded two primary observations. First, despite the effort to control the discharge characteristics of the experiment, we obtain highly variable source excitations from event-to-event (Fig. 2). Second, despite these variable source-time histories, we observe systematic variation of the spectral contents for high-quality lateral and vertical blasts (Figs. 3, 4, 5).

The near cannon spectral features carry over from the source (AC32 sensor within 2 m of the source SRC) to the outbound stations. Example waveforms and spectra for two events are shown in Fig. 3. These examples were selected because: (1) they had excellent signal-to-noise characteristics and a single broad spectral peak (2–80 Hz); (2) they represent two end member observations (both a vertical and laterally directed blast), and (3) the near source wavelets and spectra were similar for each event (Fig. 2). The waveform data for each event show approximately uniform wave pulses across the network and reveal characteristic under-sampled waveform features (Fig. 3a, b). However, the data have somewhat different event size which may contribute to the spectral observations.

For the vertically directed blast (Fig. 3a, c) the spectral characteristic on the surrounding network is strongly uniform regardless of the sensor aspect relative to the station. By comparison, the explosion having a strong lateral blast component (Fig. 3b, d) reveals systematic enrichment towards higher frequencies for sensors in the direction of the blast, and depletion of those frequencies



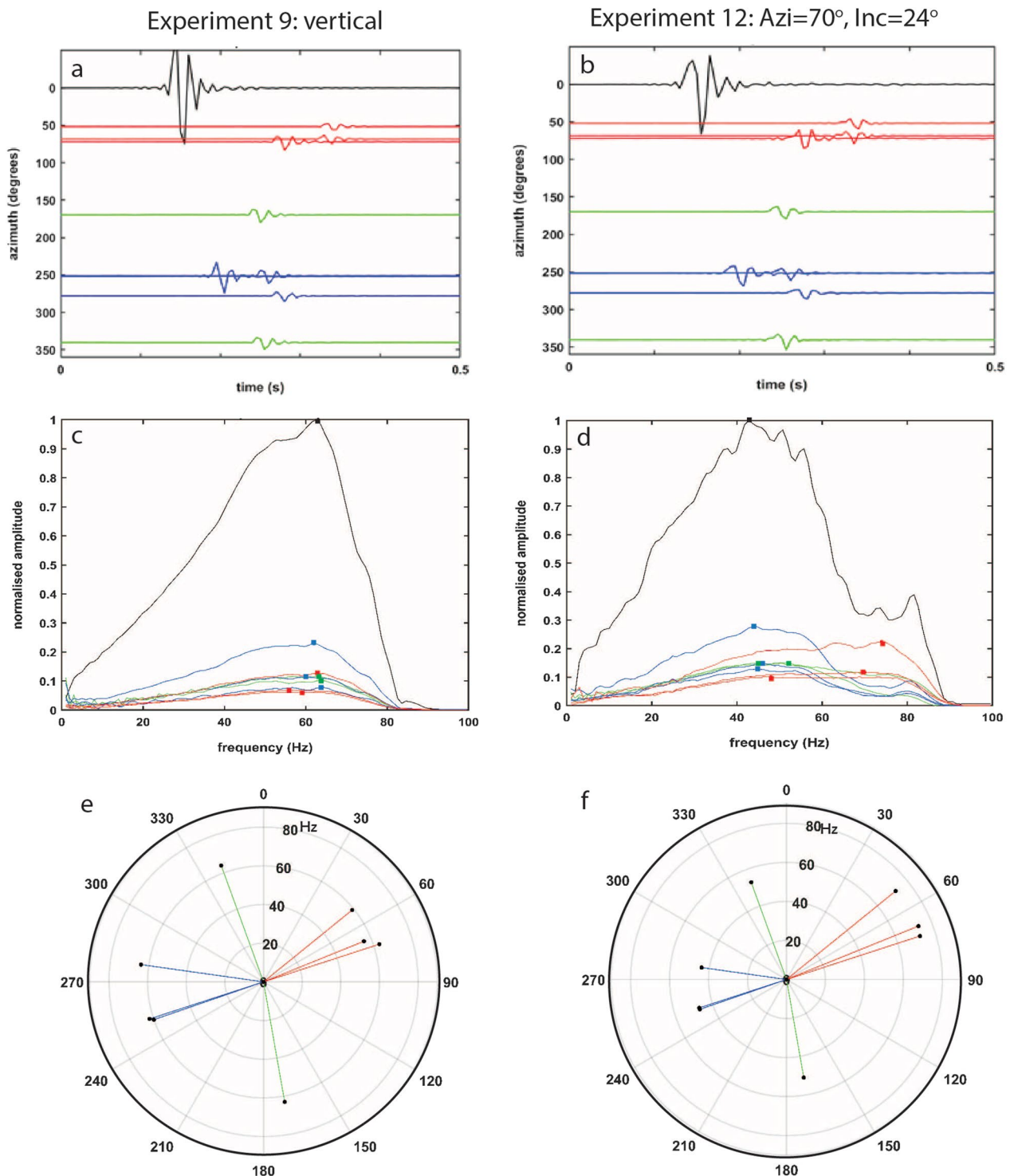


**Fig. 3** Example acoustic waveforms (**a, b**) and spectra (**c, d**) for vertical (**a, c**), and northeast-directed (**b, d**) blasts. Color is representative of the station distribution in Fig. 1. Example polar plots (**e, f**) show peak spectral frequencies (0–100 Hz with low frequencies in plot center) and station azimuth (1°–360° clockwise from North at the top) relative to the source position (SRC). Squares mark maximum frequency of each spectra as shown (**e, f**) note for lateral discharge shown in **d** and **f** the higher frequencies northeastward and diminished frequencies southwestward. The window onset for **a** and **b** is ~0.1 s prior to the explosion onset for each experiment

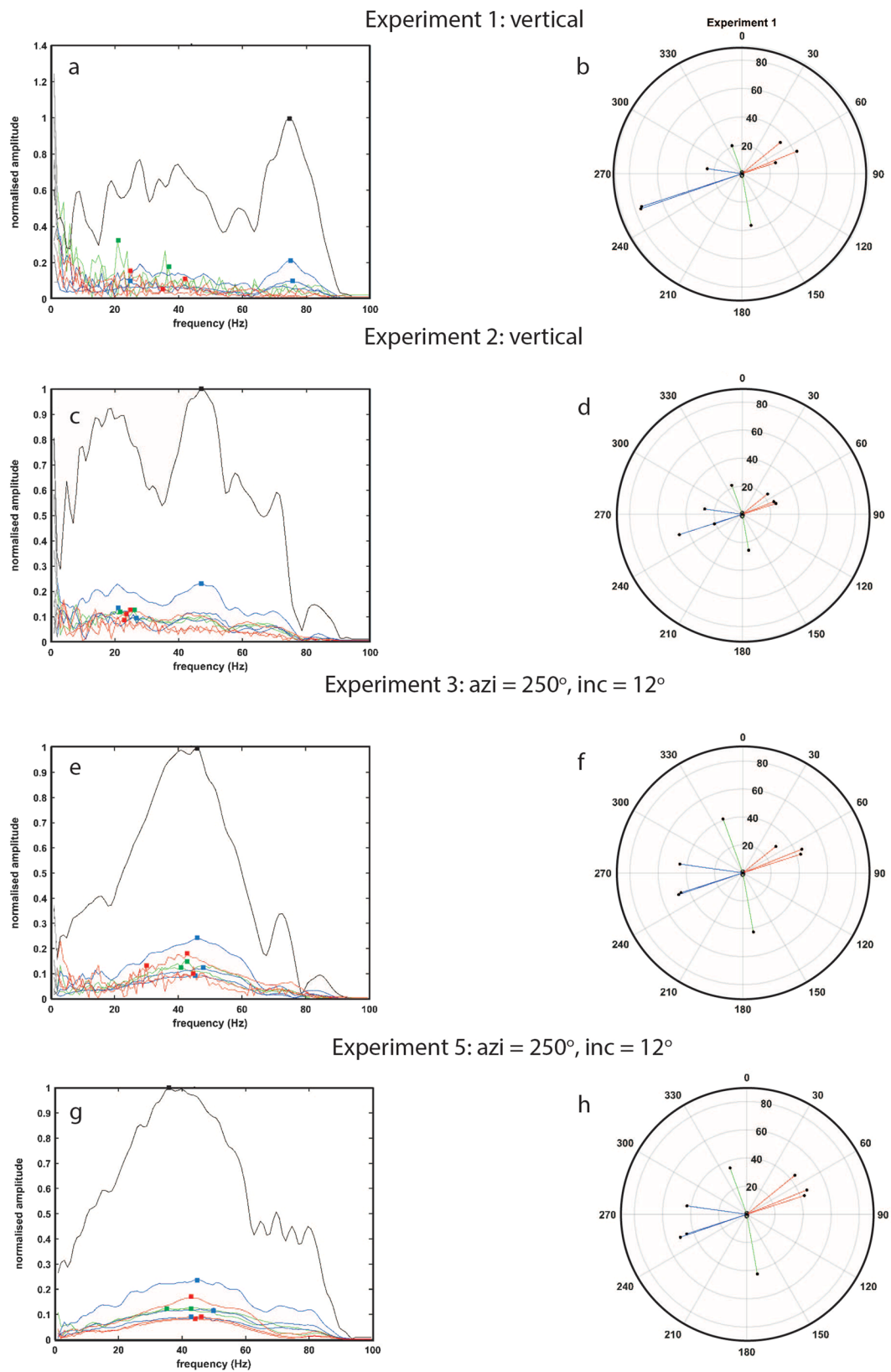


**Fig. 4** Complete analysis of eruption data for experiments 1, 2, 3, and 5 following analysis from Fig. 3



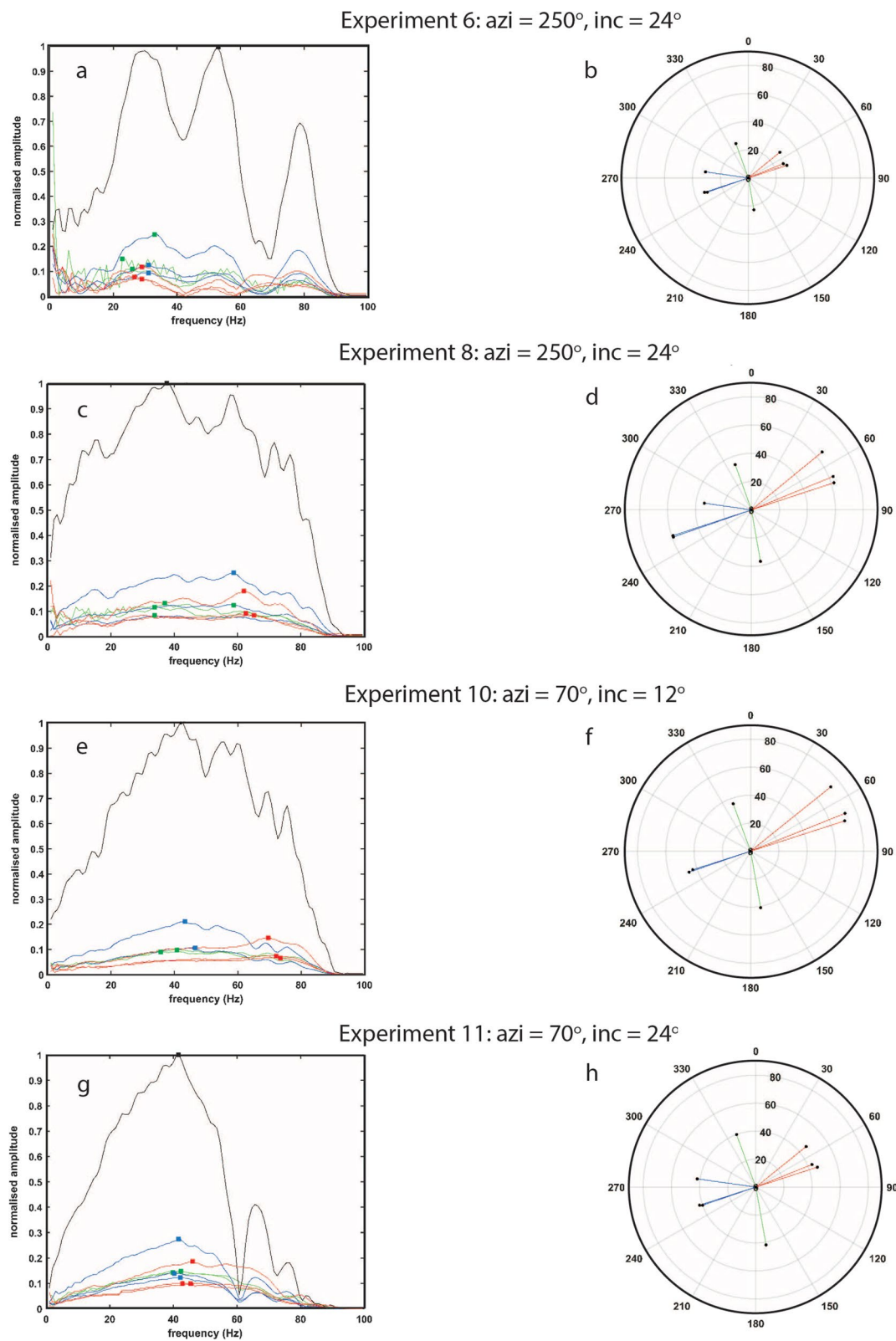


**Fig. 5** Complete analysis of eruption data for experiments 6, 8, 10 and 11 following analysis from Fig. 3

behind the blast. The observed spectral distortion occurs at  $\sim 62$  Hz for this example (see colored filled squares Fig. 3d). To illustrate the azimuthal features graphically, we plot the peak spectral frequency as a polar plot for both the vertical discharge (Fig. 3e) and the northeast-directed lateral discharge (Fig. 3f).

We see that the other 24° northeastern blast (Experiment 11-Fig. 5g, h) has somewhat similar features to Experiment 12 (Fig. 3d, f). For the smaller angle (near vertical) cannon discharges, (Experiments 3, 5 and 10 in Table 1) the systematics of lateral discharge components are not well resolved and in the case of experiment 10 (Fig. 5e, f) are similar to Experiment 11 (Fig. 5g, h). These events, along with the single vertical discharge show more uniform spectral patterns (compare Figs. 4e, g, 5e to Fig. 3c). The only southwestern directed example shows a modest frequency enrichment in the direction of the blast is seen in Experiment 5 (Fig. 4g) which has weakly enriched frequencies above 60 Hz (compare northeastward sensors (red lines) to southwestward sensors (blue lines)). Given the potential under-sampling discussed above, interpretation of higher frequency observations for this experiment should be undertaken cautiously. This assessment is completed in “Source directivity” section.

The video observations from experiment 9 show a narrow vertical explosion with a limited ballistic distribution range ( $\sim 10$  m). In contrast, experiment 12 has a northeast-directed outward fanning explosion and larger northeasterly distributed ballistic range ( $\sim 15$  m) (see Additional file 1: Supplemental Images). In all experiments, the initial measured maximum velocity of the vapor jet was higher than the subsequent measured maximum velocity of the ballistics. Experiment 9 shows that the vapor jet was higher velocity (60.0 m/s) compared to experiment 12 (28.3 m/s), consistent with the higher initial pressure calculated from the infrasound (Fig. 2), however the balls from the two experiments had similar maximum measured velocity ranges (Table 3).

## Discussion

Our results reveal highly variable source excitations from event-to-event (Fig. 2) and systematic frequency partitioning for individual events (Fig. 3c, d). These observations have implications for the interpretation of source processes that occur in a wide range of observational settings including the interpretation of repetitive sources found in both natural acoustic and seismic data (e.g., Danesi et al. 2007; Park et al. 2019).

Our experimental setup produces a source that has conceptual similarity with prior work in volcano acoustics. For example, Buckingham and Garces (1996) presented a canonical model of volcano acoustics, providing an analytic solution for the upgoing sound field from a

resonant magma (or gas-filled) conduit, with the trigger-mechanism pressure excitation function provided by a bubble pulse airgun-like source signature at depth in the conduit. We also have a submerged bubble expansion source, but in our case the wavelength of the bubble oscillations presumably approach or exceed those of the barrel container, and the bubble expansion is shallow enough that the full bubble pulse oscillations are not completed before the material is ejected. Thus, our source is more complicated than a deeper more pressure confined air-gun-like source (Buckingham and Garces 1996). Ichihara et al. (2009) discusses a related case of lake water surface explosions (not confined by conduit walls). In addition, our source is conceptually similar to the directed blast numerical simulations of Watson et al. (2021). We note that Watson et al. (2021) observed enhanced high frequencies in the downstream blast direction (i.e., above the vertically directed source), consistent with our observations.

## Variation of a repeating source

While we attempted to produce identical acoustic impulses event-to-event, strong variations in waveforms and spectra for the ten events testify to an unstable source process. This is remarkable, considering that the source location was stationary relative to the sensor array and our methodology attempted to produce a uniform source discharge. Even repeat discharges with the same cannon orientation (Experiment 11 and 12) produced somewhat different waveform and spectral characteristics (see Figs. 2, 3, 5).

In natural systems, the observed waveform is interpreted to be dominantly impacted by four elements: the source, path, site and instrument. If the source mechanism is identical for two or more events at a stationary position, then the resulting waveforms would be highly similar because each of the four elements would be nearly constant over short inter-event times (e.g., Green and Neuberg 2006; Park et al. 2019) related to a constant eruption trigger, barrel geometry, water fill level and barrel opening producing highly similar waveforms and spectra. In this context, if we return to the multi-peaked spectra for events 1, 2 and 6 (Figs. 4, 5), the observed spectral peaks might hypothetically be related to a path effect associated with a Lloyd mirror (e.g., Carey 2009) where direct and ground reflected waves might be superimposed to produce constructive and destructive wavelets dependent on the distance from the source. In our case, however, the peaks persist for all stations consistent with a source rather than path effect. Instead, the systematic similarity of all spectra for a given experiment (Figs. 4a, c, 5a) suggest that the source is dominating the

spectra and that some features experiment-to-experiment are unconstrained and highly variable.

We suggest that the non-systematic features of the experiment-to-experiment source process may relate to non-uniform strength characteristics of each plastic bottle as well as small variations in the position of the bottle at the base of the barrel. We also surmise that rapid bottle rupture would displace the bottle laterally along the base of the barrel in a somewhat random manner. The bottle rupture process may introduce unconstrained energy directivity effects. In addition, while we attempted to control the capacity of liquid nitrogen ( $N_2$ ) into each bottle, prior experiments (e.g., Wadsworth et al. 2018 and other unpublished experiments including a subset of our team) showed that larger volumes of  $N_2$  increased the explosion yield. We estimate errors in  $N_2$  bottle fill and water barrel fill to be within 5%, while the barrel inclination is known to within a couple of degrees. Finally, we note that the inclination of the barrel would produce distortions in the water height relative to the source depth. Together, these small variations probably contributed to the non-repeating rupture-time histories and attendant variation in the spectral characteristics.

In addition to the highly variable source-time histories, careful inspection of Fig. 2 suggest that waveforms may also be systematically evolving through time. We consider two aspects of the experiment that might contribute to the evolution of the waveform features. First, the bottle type was changed after the sixth experiment when the supply of L&P type bottles was exhausted. Later explosions had generally greater overpressures (Table 2) and we surmise that the MY bottles used for experiments 6–12 failed at higher internal pressure thereby initiating the expulsion event with gas at a higher pressure. Second, over the progression of the experiment, the plywood floor of the trailer began to fracture and deform. By the end of the experiment, the floor rested on the steel understructure which was also progressively deformed (Additional file 2: Fig. S1). We regard this slow destruction of the cannon's trailer frame as an analog to a destructive source process in nature although the temporal variability is difficult to constrain in our case. For the natural system, this might be equivalent to the progressive erosion of an active eruption vent (e.g., Fee et al. 2016; McNeil et al. 2018), or the progressive rupture around a repeating subsurface earthquake source (e.g., Park et al. 2019), although the experimental destructive process is not scaled, and little is known about the destructive source processes in natural systems. We regard these aspects of the experiment as the primary contributions to the large observational changes event-to-event. It is clear that care must be taken before ascribing source stability,

or progressive variations to one process or another (e.g., Park et al. 2019).

### Source directivity

Moving next to the systematic aspects of the frequency content for each event, we first examine if we have completely sampled the spectral content and, if not, what is the upper frequency that can be faithfully interpreted? For several seismic studies in volcanic settings, the interpretation is undertaken in the 2–25 Hz range for data sampled at 100 Hz (e.g., about 50% of the corresponding Nyquist frequency of 50 Hz) (e.g., Hotovec et al. 2013). In volcano observatory settings, helicopter and fixed wing aircraft noise is also commonly observed at frequencies > 10 Hz, and detailed assessments have resolved persistent signals as high as 35 Hz (Eibl et al. 2015) corresponding to about 70% of Nyquist. From this, one could anticipate that frequencies of ~70 Hz might be resolved in our 200 Hz data. However, frequency characteristics of a more persistent 'tremor like' source (e.g., a helicopter) may be easier to resolve than the short-duration impulses recovered here. Higher frequency observations may correspond to very few data samples for a given waveform in our specific case. In addition, higher frequencies might be impacted by digitizer related anti-alias filters. To assess this, we compared gain-corrected observations to poles-and-zeros restitutions to assess the high-frequency roll-off in the data (Additional file 2: Figs. S2, S3). Inspection of waveforms and spectra shows that amplitudes and frequency distortions are only seen at frequencies < ~5 Hz, as expected from the nominal response curve (Additional file 2: Fig. S4).

These considerations suggest that the frequency content of near-field acoustic sensors may be interpreted with reasonable confidence below about 70 Hz. The observed enrichment-depletion occurs around 40–70 Hz for our highest quality observations (Experiments 5, 9, 10, 11 and 12 in Fig. 2, and Figs. 4, 5, 6) while observations above 70 Hz (e.g., Experiment 5-Fig. 5g) are probably on the edge of our ability to interpret. We emphasize here the small number of experimental observations and the high variability observed event-to-event; hence a strong interpretation of the results is not possible in our case. With these caveats, we next consider the range of mechanisms that might produce the frequency enrichment observations.

The overall source dynamics for acoustic sources has been developed from early work by Woulff and McGetchin (1976) and Lighthill (1978) and consists of monopole (explosive) sources, dipole (bi-directional) sources and multipoles (superimposed combinations of dipole sources). Combinations of these source types are generally consistent with volcanic eruptions (e.g.,

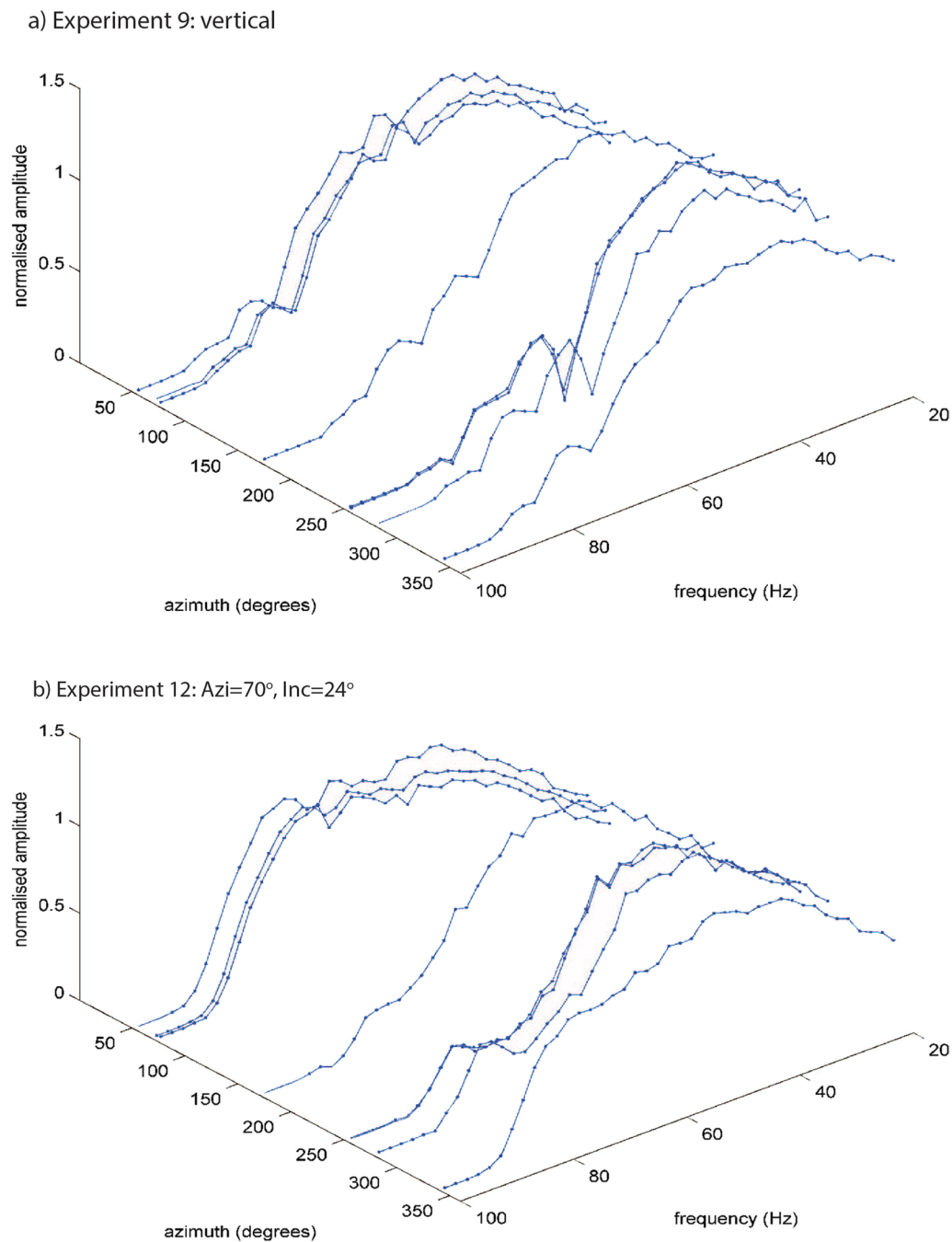


**Fig. 6** Azimuthally grouped spectra for **a** Experiment 9 and **b** Experiment 12

Iezzi et al. 2019; Kim et al. 2012) and are likely to match the observations for our experiments. In this context, we may consider the outcomes of our experiments with equivalent source representations that approximate monopole and dipole source processes (e.g., a complex source mechanism) related to directed explosions. Extending from this, we consider two possibilities for

the azimuthal enrichment: (1) frequency enhancement due to a Doppler shift of an extended source process (the source and its extended plume), or (2) a diffraction of acoustic wave energy due to the obstruction of the cannon barrel and trailer bed. Other contributions to variable source spectral observations might include

variable water height in the inclined barrel or systematic shifts in the explosive source at the base. Such effects are hard to assess within this contribution and are not considered further.

#### **Plume energetics and the Doppler shift**

In the first case, we assume that the acoustic source propagates at subsonic speeds and that the source includes both the initial rupture and expansive discharge, but also a distributed source component representing the ejected plume. The acoustic source is confined and directed from the barrel itself and propagates outward with an efficiency related to the visco-elastic barrel base and walls as well as the opening. We envisage that the barrel is the primary source, but the mass of the ejected fluids may produce acoustic signals by plume turbulence (e.g., Matoza et al. 2009, 2013). From an observational perspective water,  $N_2$  gas and colored balls are clearly directed by the barrel orientation. The system may be analogous to water/gas explosions in laboratory settings (Ichihara et al. 2009; Zhang et al. 2016) and also for acid lake hydrothermal eruptions (e.g., Caudron et al. 2018; Jolly et al. 2018). We hypothesize that this system would produce enriched frequencies in the direction of plume propagation, and depleted frequencies behind the plume.

To test this hypothesis, we examined the discrete motions of discharged particles using methods outlined in Jolly et al. (2016). For this purpose, we tracked both individual-colored balls contained in the water as well as individual steam propagation fronts using video data. For the balls, the estimated velocity was about 10–20 m/s while the water splash and  $N_2$  gas mixture was found to have a velocity around 28–60 m/s. We note that the balls have lower density and larger volume compared to the individual water splashes mixture, producing increased frictional drag that likely contributed to their observed lower maximum velocities. It is also worth noting that the balls tended to be measured farther along their trajectories away from the source, whereas the water gas jet was measured closer to source (see supplementary videos and Table 3).

Restricting our analysis to the steam propagation and assuming that the plume is the source of mass propagation producing the full infrasound waveform, we use the standard formulation for the Doppler shift,  $F_t = f_o(C + V_r)/(C - V_s)$ , for propagation towards the observation point, and  $F_a = f_o(C - V_r)/(C + V_s)$ , for propagation away from the observation point. Here  $f_o$  is the frequency of the source,  $V_s$  is the velocity of the propagating source,  $V_r$  is the velocity of the stationary receiver (0 m/s),  $C$  is the acoustic velocity which is assumed 345 m/s. Because the angled source includes both vertical and lateral velocity components, we apply a Cartesian

correction to obtain the lateral component along the Earth's surface. For the maximum amplitude for Experiment 12 ( $f_o \sim 45$  Hz at the near source station AC32) we obtain  $F_a = 43.5$  Hz and  $F_t = 46.6$  Hz. The observed range of frequencies is 43 Hz (blue lines in Fig. 3d) and 73 Hz (red lines in Fig. 3d). While the theoretical Doppler shift is of the correct polarity and may partially contribute to the observations, the Doppler-related frequency distortion is not sufficient to produce the acoustic observations in Fig. 3. While it is likely that the discharge velocities within the cannon barrel are more than those observed in the video, a Doppler shift cannot fully explain the observations for Experiment 12.

#### **Wave diffraction and frequency content**

An alternative hypothesis is that the cannon and trailer may produce a natural barrier to the propagation of acoustic energy within the sampled frequency range (e.g., Kim et al. 2012). For a vertical discharge, all frequencies are propagated uniformly, producing the observations shown in Fig. 3c. With increased lateral discharge, the sensors open to the barrel would have no barrier to the full spectral content of the discharge, while sensors laterally and behind the cannon would record diffracted acoustic signals, with these effects being more pronounced at higher frequencies. In this case, the laterally directed energy from the barrel would produce some recoil energy that is partially absorbed and distributed by the barrel walls, trailer, and other elements like rubber wheels, shock absorbers and the ground. We observed recoil and barrel bounce associated with all discharges, and distinct late arriving acoustic transients at the near source station (see Additional file 2: Fig. S5). While we were able to document lag times from the video records that may relate to pressure transients at the near source sensor (AC32), a lack of absolute timing for video records implies inexact measurement of lag times. Regardless, we find lag times from 0.2 (experiment 5) to 0.9 s (experiment 9) after the visible initiation of the experiment.

It is difficult to test the wave diffraction hypothesis, without application of synthetic waveform modeling incorporating elastic or visco-elastic boundaries. While modeling for directed sources in active volcanoes has been completed based on a stationary source with directionality represented by a force vector (e.g., Iezzi et al. 2019), such modeling would be difficult to implement in our case given the scale issues and complexity of the apparatus. Regardless, we surmise that both the extended distributed source model, and the visco-elastic barrier model likely contribute to our observations.



## Conclusions and implications

This work highlights the observations from vertical and laterally directed explosions from an experimental apparatus designed to emulate natural phenomena from volcanic eruptions. Our primary observations include strongly variable source time functions for waveforms and spectra as part of a spatially distributed source process and frequency enrichment/depletion profiles associated with laterally directed blast events.

Limitations in the initial experimental design have been highlighted to aid the interpretation of the data as well as to highlight possible improvements to future experiments of this type. Among these, we note the possible under-sampling of the experiment and its potential impacts on our interpretations. While we acknowledge that the observed waveforms and spectra may not represent the full wavefield, we note that the observations are systematically seen on multiple stations and azimuthal directions. In this regard, future experiments of this type should increase the sampling rate to at least 400 Hz. While this is within the specification for the infraBSU and CUBE digitizer, microphone-based recording may improve resolution of high-frequency components. In addition, application of a different cannon design might improve the observational range that could be assessed. For example, use of a cannon apparatus incorporating solid chemical explosive sources (e.g., Goto et al. 2001; Bowman et al. 2014; Sonder et al. 2022), could produce more uniform discharges at greater inclinations. While the use of chemical explosives increases logistical complexity and expense, they would allow assessment of 'dry bed' lateral eruption dynamics. Dry-bed eruptions might also be simulated using the same liquid nitrogen-charged cannon but excluding the confining water column. Further, denser observation including more acoustic sensors at a greater range of azimuths and incidence angles, would potentially allow incorporation of more sophisticated modeling approaches as well as the application of source inversion. While such approaches may be beyond the applicability of the present data, a new experiment including dense ground and aerial deployments (e.g., Jolly et al. 2017) could allow a more rigorous assessment of extended source processes. In addition, it would be useful to incorporate video records having absolute timing, as this would improve assessment of late-stage secondary pulses (Additional file 2: Fig. S5). The largest secondary pulse, for experiment 6, was observed clearly across all sensors in the local network.

Results from this experiment illustrate that variations in the energy release from angled explosions can be captured in acoustic sensors surrounding volcanic systems. The observed acoustic spectra varied considerably between experiments despite similar experimental

setups and an effort to have a repeatable source, suggesting that small changes in source dynamics can produce large observed changes in the acoustics in this experimental setup. While the observations were collected from very near source, where the source dimension is large compared to the observation network, they offer an immediate applicability to improved volcano eruption assessments. In particular, the results highlight the potential for dense near-field capture of volcanic eruption data for frequently active phreatic or Strombolian systems, where localized hazards may be present. Such observations may enable the development of improved hazards zones for emergency managers, and improved eruption detection systems for volcano monitoring akin to mass motion monitoring systems for lahar monitoring systems (e.g., Sanderson et al. 2021).

## Supplementary Information

The online version contains supplementary material available at <https://doi.org/10.1186/s40623-022-01732-0>.

**Additional file 1. Video:** Example video showing cannon discharge particle tracking.

**Additional file 2. Fig. S1:** Image showing damage to cannon trailer. **Fig. S2:** Comparison between gain corrected (blue) acoustic waveforms and poles and zeros corrected waveforms (red) for experiment 9. **Fig. S3:** Gain corrected spectra (blue) compared to poles and zeros corrected spectra (red) for experiment 9. Note the strong match in observations above 10 Hz. **Fig. S4:** Nominal response curve for infraBSU/CUBE system. Note the strong sensitivity roll-off > 80 Hz. **Fig. S5:** Secondary pulse (arrows) observed for a subset of cannon discharge events.

## Acknowledgements

We acknowledge the New Zealand Ministry of Business, Innovation and Employment (MBIE) who supported AJ (formerly with GNS Science), BK, BC, RJ and Cam Asher and the New Zealand MBIE funded program Resiliency to Natures Challenges for support of BK and AJ (formerly with GNS Science). RSM acknowledges NSF grant EAR-1847736. NSF Grant EAR-1952392 supported AMI (UCSB). DF acknowledges support from NSF Grant EAR-1901614. Julian Thompson and Cam Asher provided video support of the project (GNS Science). We thank Leighton Watson for discussion about numerical simulations of explosions and Iseul Park for discussions around response correction for acoustic data. This manuscript was improved by reviews by Alicia Hotovec-Ellis and two anonymous reviewers. Finally, we thank handling editor Mie Ichihara for guiding the submission and very useful suggestions to improve the manuscript. Any use of trade, firm, or product names is for descriptive purposes only and does not imply endorsement by the U.S. Government.

## Author contributions

AJ and BK conceptualized the experiment. RJ provided engineering and logistical support. AJ, BK, BC and RJ conducted the experiment. AJ, RM and AI processed and analyzed the acoustic data. AS, BK and AJ analyzed the video records. All authors supported the writing and approved the final manuscript.

## Funding

New Zealand Ministry of Business, Innovation and Employment (MBIE) who supported AJ (formerly with GNS Science), BK, BC, RJ and CA and the New Zealand MBIE funded program Resiliency to Natures Challenges for support of BK and AJ (formerly with GNS Science). NSF Grant EAR-1952392 supported AMI.

## Availability of data and materials

Acoustic and video data used in this study are available as supplemental downloads including: four gifs are supplied from camera 2, two for each experiment (both the tracked vapor jet and the tracked balls). Inverted color images in most cases provided the best contrast except for in the case of tracking the vapor jet in experiment 12 due to lighting. And raw video footage is available on the ScienceBase open access service: Jolly, A.D., and Kennedy, B., 2022, Video Data for Cannon Discharge Events—May 3, 2016—Taupo, New Zealand: U.S. Geological Survey data release, <https://doi.org/10.5066/P92KGW45>. Waveform data are available through the IRIS temporary network code 7L [https://www.fdsn.org/networks/detail/7L\\_2016/](https://www.fdsn.org/networks/detail/7L_2016/).

## Declarations

### Ethics approval and consent to participate

Not applicable.

### Consent for publication

This publication has been peer reviewed and approved for publication consistent with U.S. Geological Survey Fundamental Science Practices (<https://pubs.usgs.gov/circ/1367/>).

### Competing interests

Arthur D. Jolly is a member of the EPS editorial board and is blinded to the editorial process. The other authors declare that they have no competing interests.

### Author details

<sup>1</sup>U.S. Geological Survey, Hawaiian Volcano Observatory, Suite A8, 1266 Kamehameha Avenue, Hilo, HI 96720, USA. <sup>2</sup>GNS Science, 1 Fairway Drive, Avalon, Lower Hutt 5010, New Zealand. <sup>3</sup>Department of Geological Sciences, University of Canterbury, Christchurch, New Zealand. <sup>4</sup>Department of Earth Science and Earth Research Institute, University of California, Santa Barbara, CA, USA. <sup>5</sup>GNS Science, Gracefield, New Zealand. <sup>6</sup>GNS Science, Wairakei Research Centre, 114 Karetoto Rd., Wairakei, New Zealand. <sup>7</sup>Alaska Volcano Observatory, Geophysical Institute, University of Alaska, Fairbanks, USA. <sup>8</sup>U.S. Geological Survey, Cascades Volcano Observatory, 1300 SE Cardinal Ct., WA 98683 Vancouver, United States.

Received: 15 February 2022 Accepted: 2 November 2022

Published online: 02 December 2022

## References

- Abercrombie RE, Poli P, Bannister S (2017) Earthquake directivity, orientation, and stress drop within the subducting plate at the Hikurangi margin, New Zealand. *J Geophys Res: Solid Earth* 122:12176–10188. <https://doi.org/10.1002/2017JB014935>
- Bowman DC, Taddeucci J, Kim K, Anderson JF, Lees JM, Graettinger AH, Sonder I, Valentine GA (2014) The acoustic signatures of ground acceleration, gas expansion, and spall fallback in experimental volcanic explosions. *Geophys Res Letts* 41:1916–1922. <https://doi.org/10.1002/2014GL059324>
- Buckingham MJ, Garcés MA (1996) Canonical model of volcano acoustics. *J Geophys Res* 101(B4):8129–8151. <https://doi.org/10.1029/95JB01680>
- Carey WM (2009) Lloyds mirror-image interference effects. *Acoust Today*, April, 14–20
- Caudron C, Taisne B, Neuberg J, Jolly AD, Christenson BW, Lecocq T, Suparjan SD, Suantika G (2018) Anatomy of phreatic eruptions. *Earth Planets Space* 70:168. <https://doi.org/10.1186/s40623-018-0938-x>
- Danesi S, Bannister S, Morelli A (2007) Repeating earthquakes from rupture of an asperity under an Antarctic outlet glacier. *Earth Planet Sci Letts* 253:151–158. <https://doi.org/10.1016/j.epsl.2006.10.023>
- Eberhart-Phillips D et al (2003) The 2002 Denali Fault Earthquake, Alaska: A large magnitude, Slip-Partitioned Event. *Science*. <https://doi.org/10.1126/science.1082703>
- Eibl EPS, Lokmer I, Bean CJ, Akerlie E, Vogtford KS (2015) Helicopter vs. volcanic tremor: characteristic features of seismic harmonic tremor on volcanoes. *J Volcanol Geotherm Res* 304:108–117. <https://doi.org/10.1016/j.jvolgeoes.2015.08.002>
- Erfurt-Cooper P (ed) (2014) Volcanic tourist destinations. Springer, London. <https://doi.org/10.1007/978-3-642-16191-9>
- Fee D, Haney MM, Matoza RS, Van Eaton AR, Cervelli P, Schneider DJ, Iezzi AM (2016) Volcanic tremor and plume height hysteresis from Pavlof Volcano, Alaska. *Science* 355(6320):45–48. <https://doi.org/10.1126/science.aah6108>
- Fee D, Lyons J, Haney M, Wech A, Waythomas C, Diefenbach AK et al (2020) Seismo-acoustic evidence for vent drying during shallow submarine eruptions at Bogoslof volcano, Alaska. *Bull Volcanol* 82(1):2. <https://doi.org/10.1007/s00445-019-1326-5>
- Fitzgerald RH, Tsunematsu K, Kennedy BM, Breard E, Lube G, Wilson TM, Jolly AD, Pawson J, Rosenberg MD, Cronin SJ (2014) The application of a calibrated 3D ballistic trajectory model to ballistic hazard assessments at Upper Te Maari, Tongariro. *J Volcanol Geotherm Res* 286:248–262. <https://doi.org/10.1016/j.jvolgeoes.2014.04.006>
- Fitzgerald RH, Kennedy BM, Wilson TM, Leonard GS, Tsunematsu K, Keys H (2017) The communication and risk management of volcanic ballistic hazards advances in volcanol. Springer, London, pp 121–147. [https://doi.org/10.1007/1157\\_2016\\_35](https://doi.org/10.1007/1157_2016_35)
- Fitzgerald RH, Kennedy BM et al (2020) Volcanic ballistic projectile deposition from a continuously erupting volcano: Yasur Volcano, Vanuatu. *Volcanica* 3(2):183–204. <https://doi.org/10.30909/vol.03.02.183204>
- Goto A, Taniguchi H, Yoshida M, Ohba T, Oshima H (2001) Effects of explosion energy and depth to the formation of blast wave and crater: field explosion experiment for the understanding of volcanic explosion. *Geophys Res Letts* 28(22):4287–4290. <https://doi.org/10.1029/2001GL013213>
- Green DN, Neuberg J (2006) Waveform classification of volcanic low-frequency earthquakes swarms and its implication at Soufrière Hills Volcano, Montserrat. *J Volcanol Geotherm Res* 153(1–2):51–63. <https://doi.org/10.1016/j.jvolgeoes.2005.08.003>
- Hotovec AJ, Prejahn SG, Vidale JE, Gombert J (2013) Strongly gliding harmonic tremor during the 2009 eruption of Redoubt Volcano. *J Volcanol Geotherm Res* 259:89–99. <https://doi.org/10.1016/j.jvolgeoes.2012.01.001>
- Hubbard HH, Lansing D, Runyan H (1971) A review of Blade Noise Technology. *J Sound Vib* 19(3):227–249. [https://doi.org/10.1016/0022-460X\(71\)90686-9](https://doi.org/10.1016/0022-460X(71)90686-9)
- Ichihara M, Ripepe M, Goto A, Oshima H, Aoyama H, Iguchi M, Tanaka K, Taniguchi H (2009) Airwaves generated by an underwater explosion: implications for volcanic infrasound. *J Geophys Res* 114:B03210. <https://doi.org/10.1029/2008JB005792>
- Iezzi AM, Fee D, Kim K, Jolly AD, Matoza RS (2019) Three-dimensional acoustic multipole waveform inversion at Yasur Volcano, Vanuatu. *J Geophys Res: Solid Earth* 124(8):8679–8703. <https://doi.org/10.1029/2018JB017073>
- Jolly AD, Sherburn S, Jousset P, Kilgour G (2010) Eruption source processes derived from seismic and acoustic observations of the 25 September 2007 Ruapehu eruption—North Island, New Zealand. *J Volcanol Geotherm Res* 191:33–45. <https://doi.org/10.1016/j.jvolgeoes.2010.01.009>
- Jolly AD, Jousset P, Lyons JJ, Carniel R, Fournier N, Fry B, Miller C (2014) Seismoacoustic evidence for an avalanche driven phreatic eruption through a beheaded hydrothermal system: an example from the 2012 Tongariro eruption. *J Volcanol and Geotherm Res* 286:331–347. <https://doi.org/10.1016/j.jvolgeoes.2014.04.007>
- Jolly A, Kennedy B, Edwards M, Jousset P, Scheu B (2016) Infrasound tremor from bubble burst eruptions in the viscous shallow crater lake of White Island, New Zealand, and its implications for interpreting volcanic source processes. *J Volcanol Geotherm Res* 327:585–603. <https://doi.org/10.1016/j.jvolgeoes.2016.08.010>
- Jolly AD, Matoza RS, Fee D, Kennedy BM, Iezzi AM, Fitzgerald RH et al (2017) Capturing the acoustic radiation pattern of Strombolian eruptions using infrasound sensors aboard a tethered aerostat, Yasur volcano, Vanuatu. *Geophys Res Letts* 44:9672–9680. <https://doi.org/10.1002/2017GL074971>
- Jolly A, Lokmer I, Christenson B, Thun J (2018) Relating gas ascent to eruption triggering for the April 27, 2016, White Island (Whakaari), New Zealand eruption sequence. *Earth Planets Space* 70:177. <https://doi.org/10.1186/s40623-018-0948-8>
- Kanamori H, Given JW (1982) Analysis of long-period seismic waves excited by the May 18, 1980, eruption of Mount St. Helens—A terrestrial monopole? *J Geophys Res* 82(B7):5422–5432. <https://doi.org/10.1029/JB087iB07p05422>
- Kieffer SW (1981) Blast dynamics at Mount St. Helens on 18 May 1980. *Nature* 291:568–570. <https://doi.org/10.1038/291568a0>

- Kilgour G, Manville V, Della Pasqua F, Graettinger A, Hodgson KA, Jolly GE (2010) The 25 September 2007 eruption of Mount Ruapehu, New Zealand: directed ballistics, surtseyan jets, and ice-slurry lahars. *J Volcanol Geotherm Res* 191:1–14. <https://doi.org/10.1016/j.jvolgeores.2009.10.015>
- Kilgour G, Kennedy B, Scott B, Christenson B, Jolly A, Asher C, Rosenberg M, Saunders K (2021) Whakaari/White Island: a review of New Zealand's most active volcano, New Zealand. *J of Geol and Geophys* 64(2–3):273–295. <https://doi.org/10.1080/00288306.2021.1918186>
- Kim K, Lees JM, Ruiz M (2012) Acoustic multipole source model for volcanic explosions and inversion for source parameters. *Geophys J Int* 191(3):1192–1204. <https://doi.org/10.1111/j.1365-246X.2012.05696.x>
- Lighthill J (1978) *Waves in fluids*, 2nd edn. Cambridge University Press, Cambridge
- Lube G, Breard ECP, Cronin SJ, Proctor JN, Brenna M, Moebis A et al (2014) Dynamics of surges generated by hydrothermal blasts during the 6 August 2012 Te Maari eruption, Mt. Tongariro, New Zealand. *J Volc Geotherm Res* 286:348–366. <https://doi.org/10.1016/j.jvolgeores.2014.05.010>
- Lyons JJ, Haney MM, Fee D, Wech AG, Waythomas CF (2019) Infrasound from giant bubbles during explosive submarine eruptions. *Nature Geosci* 12(11):952–958. <https://doi.org/10.1038/s41561-019-0461-0>
- Marcillo O, Johnson JB, Hart D (2012) Implementation, characterization, and evaluation of an inexpensive low-power low-noise infrasound sensor based on a micromachined differential pressure transducer and a mechanical filter. *J Atmos Ocean Tech*. <https://doi.org/10.1175/JTECH-D-11-00101.1>
- Matoza RS, Garces MA, Chouet BA, D'Auria L, Hedlin MAH, De Groot-Hedlin C, Waite GP (2009) The source of infrasound associated with long-period events at Mount St. Helens. *J Geophys Res: Solid Earth* 114:B04305. <https://doi.org/10.1029/2008JB006128>
- Matoza RS, Fee D, Neilsen TB, Gee K, Ogden DE (2013) Aeroacoustics of volcanic jets: Acoustic power estimation and jet velocity dependence. *J Geophys Res: Solid Earth* 118:6269–6284. <https://doi.org/10.1002/2013JB010303>
- McNeal JS, Jones J, Cal RB, Mastin LG, Kim D, Solovitz SA (2018) Experimental study of analogue vent erosion towards nozzle shapes. *J Volcanol Geotherm Res* 367:79–87. <https://doi.org/10.1016/j.jvolgeores.2018.10.022>
- Park I, Jolly A, Kim KY, Kennedy B (2019) Temporal variations of repeating low frequency volcanic earthquakes at Ngauruhoe Volcano, New Zealand. *J Volcanol Geotherm Res* 373:108–119. <https://doi.org/10.1016/j.jvolgeores.2019.01.024>
- Rowell CR, Fee D, Szuberla CA, Arnoult K, Matoza RS, Firstov PP et al (2014) Three-dimensional volcano-acoustic source localization at Karymsky Volcano, Kamchatka, Russia. *J Volcanol Geotherm Res* 283:101–115. <https://doi.org/10.1016/j.jvolgeores.2014.06.015>
- Sanderson RW, Matoza RS, Haymon RM, Steidl JH (2021) A pilot experiment on infrasonic lahar detection at Mount Adams, Cascades: ambient infrasound and wind-noise characterization at a quiescent stratovolcano. *Seis Res Lett* 92(5):3065–3086. <https://doi.org/10.1785/0220200361>
- Sonder I, Graettinger A, Neilsen TB, Matoza RS, Taddeucci J, Oppenheimer J, Lev E, Tsunematsu K, Waite G, Valentine GA, Befus KS (2022) Experimental multiblast craters and ejecta—seismo-acoustics, jet characteristics, craters, and ejecta deposits and implications for volcanic explosions. *J Geophys Res Solid Earth* 127:e2022JB023952. <https://doi.org/10.1029/2022JB023952>
- Takarada S, Oikawa T, Furukawa R et al (2016) Estimation of total discharged mass from the phreatic eruption of Ontake Volcano, central Japan, on September 27, 2014. *Earth Planets Space* 68:138. <https://doi.org/10.1186/s40623-016-0511-4>
- Tsunematsu K, Ishimine Y, Kaneko T et al (2016) Estimation of ballistic block landing energy during 2014 Mount Ontake eruption. *Earth Planets Space* 68:88. <https://doi.org/10.1186/s40623-016-0463-8>
- Wadsworth FB, Unwin HE et al (2018) Trashcano: developing a quantitative teaching tool to understand ballistics accelerated by explosive volcanic eruptions. *Volcanica* 1(2):107–126. <https://doi.org/10.30909/vol.01.02.107126>
- Watson LM, Dunham EM, Mohaddes D, Labahn J, Jaravel T, Ihme M (2021) Infrasound radiation from impulsive volcanic eruptions: nonlinear aeroacoustic 2D simulations. *J Geophys Res: Solid Earth* 126:e2021JB021940. <https://doi.org/10.1029/2021JB021940>
- Woulff G, McGetchin T (1976) Acoustic noise from volcanoes: theory and experiment. *Geophys J Roy Astron Soc* 45:601–616. <https://doi.org/10.1111/j.1365-246X.1976.tb06913.x>
- Zhang L, Wang H, Ruan W (2016) Experiments on jet noise reduction with a liquid column. *Acoust Aust* 44:291–297. <https://doi.org/10.1007/s40857-016-0056-5>

## Publisher's Note

Springer Nature remains neutral with regard to jurisdictional claims in published maps and institutional affiliations.

**Submit your manuscript to a SpringerOpen<sup>®</sup> journal and benefit from:**

- Convenient online submission
- Rigorous peer review
- Open access: articles freely available online
- High visibility within the field
- Retaining the copyright to your article

---

Submit your next manuscript at ► [springeropen.com](https://www.springeropen.com)